

MIT Open Access Articles

Electrokinetic properties of the mammalian tectorial membrane

The MIT Faculty has made this article openly available. **Please share** how this access benefits you. Your story matters.

Citation: Ghaffari, R., S. L. Page, S. Farrahi, J. B. Sellon, and D. M. Freeman. "Electrokinetic properties of the mammalian tectorial membrane." *Proceedings of the National Academy of Sciences* 110, no. 11 (March 12, 2013): 4279-4284.

As Published: <http://dx.doi.org/10.1073/pnas.1214744110>

Publisher: National Academy of Sciences (U.S.)

Persistent URL: <http://hdl.handle.net/1721.1/80716>

Version: Final published version: final published article, as it appeared in a journal, conference proceedings, or other formally published context

Terms of Use: Article is made available in accordance with the publisher's policy and may be subject to US copyright law. Please refer to the publisher's site for terms of use.



Electrokinetic properties of the mammalian tectorial membrane

Roozbeh Ghaffari^{a,b}, Scott L. Page^{a,c}, Shirin Farrahi^{a,c}, Jonathan B. Sellon^{a,b}, and Dennis M. Freeman^{a,b,c,d,1}

^aResearch Laboratory of Electronics, Massachusetts Institute of Technology, Cambridge, MA 02139; ^bHarvard–MIT Division of Health Sciences and Technology, Cambridge, MA 02139; ^cDepartment of Electrical Engineering and Computer Science, Massachusetts Institute of Technology, Cambridge, MA 02139; and ^dEaton-Peabody Laboratory of Auditory Physiology, Massachusetts Eye and Ear Infirmary, Boston, MA 02114

Edited by Paul Albert Fuchs, The Johns Hopkins University School of Medicine, Baltimore, MD, and accepted by the Editorial Board January 29, 2013 (received for review August 28, 2012)

The tectorial membrane (TM) clearly plays a mechanical role in stimulating cochlear sensory receptors, but the presence of fixed charge in TM constituents suggests that electromechanical properties also may be important. Here, we measure the fixed charge density of the TM and show that this density of fixed charge is sufficient to affect mechanical properties and to generate electrokinetic motions. In particular, alternating currents applied to the middle and marginal zones of isolated TM segments evoke motions at audio frequencies (1–1,000 Hz). Electrically evoked motions are nanometer scaled (~5–900 nm), decrease with increasing stimulus frequency, and scale linearly over a broad range of electric field amplitudes (0.05–20 kV/m). These findings show that the mammalian TM is highly charged and suggest the importance of a unique TM electrokinetic mechanism.

cochlear amplification | cochlear mechanics | mechanoelectrical transduction | motility

The mammalian cochlea is a remarkable sensor capable of detecting and analyzing sounds that generate subatomic vibrations (1). This extraordinary sensing property depends on mechanoelectrical transduction (MET) of cochlear hair cells (2, 3), which are functionally classified as inner and outer hair cells (OHCs). Both types of hair cells project stereociliary hair bundles from their apical surface toward an overlying extracellular matrix called the tectorial membrane (TM). Because of its strategic position above the hair bundles, the TM is believed to play a critical role in bundle deflection. Recently, genetic studies confirmed the importance of the TM in hair cell stimulation by highlighting how mutations of TM proteins cause severe hearing deficits, even when the TM and its structural attachments appear to be normal under electron microscopy (4–8).

Despite significant evidence establishing the importance of the TM in normal cochlear function, relatively little is known about the TM's basic physicochemical properties and mechanistic role. Historically, models of cochlear function have represented the TM as a stiff lever with a compliant hinge, as a resonant mass-spring system, or as an inertial body (9–16). However, these models exclude important phenomena, such as longitudinal coupling (17–20), and assume that only mechanical properties of the TM are important. It now is clear that the TM is a biphasic poroelastic tissue (21), which manifests longitudinal coupling in the form of traveling waves (18–20).

Furthermore, TM macromolecules comprise not only mechanical constituents (21–26) such as collagen fibrils, but also charged constituents such as glycosaminoglycans (GAGs), which might affect mechanical properties (Fig. 1) (27–35). GAGs in the TM carry sulfate (SO_3^-) and carboxyl (COO^-) charge groups, which are fully ionized at physiological pH and neutralized at acidic pH values (pKs between 2 and 4) (27). In contrast, the net charge on TM collagen constituents is small at physiological pH because the net charge of amino (NH_3^+) and carboxyl groups is zero. The density of TM charged macromolecules previously was inferred from pH-dependent volume measurements of the TM (36–38). Although consistent with a gel model of the TM, estimates of

charge density based on changes in volume are indirect and deviate from model predictions at low pHs (38). More direct electrical recordings thus are required to determine the net charge of TM constituents and to determine whether this amount of charge is sufficient to generate electromechanical behaviors of the type reported in other connective tissues, such as cartilage (39–41).

Fixed charge plays a key role in determining the functional properties of cartilage. For example, nearly half the load-bearing stiffness of cartilage has been attributed to electrostatic repulsion (34). In addition, mechanical strain produces electrical responses [e.g., streaming potentials (35)], and electrical stimulation may lead to mechanical deformations by a process referred to as electrokinetics (39, 40). The similarity between the structure and composition of the TM and those of other connective tissues suggests the possibility that charge might play a similarly important role in the function of the TM (27, 28).

In this study, we developed microfabricated devices that interface with the soft and fragile structure of fresh, excised TM segments to (i) measure the fixed charge density of the TM and (ii) apply oscillatory electric fields at audio frequencies to the TM. Using these methodologies, we demonstrate electrokinetic phenomena elicited by the presence of fixed charge and suggest implications for hearing mechanisms.

Results and Discussion

To determine the fixed charge concentration of the TM, we recorded the electrical responses of the TM using a microaperture chamber in a patch clamp configuration (Fig. 2; *Materials and Methods*). The voltage measured between the baths represents the sum of the junction potentials at two TM surfaces (Fig. 2*A* and *B*): one bathed in artificial endolymph (AE) and one bathed in a test solution. KCl concentration in the test solution was altered systematically to modulate the adjacent junction potential via changes in charge shielding. The resulting measurements were well fit by a model based on the Donnan relation (*Materials and Methods*) and provided an estimate of fixed charge density c_f of -7.1 ± 2.0 mmol/L at physiological pH, and 3.0 mmol/L at pH 3.5 (Fig. 2*C*). These results are consistent with predictions based on biochemical composition studies (27). The net charge of approximately -7.1 mmol/L at physiological pH is large, representing 1 fixed charge molecule for every ~ 25 cations in endolymph.

To determine the mechanical contribution of charge in the TM, we analyzed a macrocontinuum model based on the stress–strain relation and Donnan equilibrium (27, 41). Internal pressures that

Author contributions: R.G., S.L.P., and D.M.F. designed research; R.G., S.L.P., S.F., and J.B.S. performed research; R.G., S.L.P., S.F., and J.B.S. analyzed data; and R.G. and D.M.F. wrote the paper.

The authors declare no conflict of interest.

This article is a PNAS Direct Submission. P.A.F. is a guest editor invited by the Editorial Board. Freely available online through the PNAS open access option.

¹To whom correspondence should be addressed. E-mail: freeman@mit.edu.

This article contains supporting information online at www.pnas.org/lookup/suppl/doi:10.1073/pnas.1214744110/-DCSupplemental.

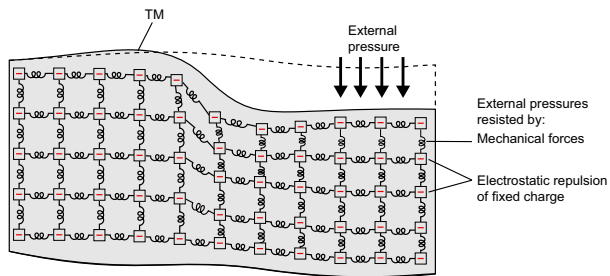


Fig. 1. Electromechanical properties of the TM. Schematic drawing of the TM showing negative fixed-charge constituents attached to a network of mechanical springs (collagen fibers). In response to external pressure, the negative fixed charge and collagen fibers resist compression through electrostatic repulsion effects and mechanical forces, respectively.

arise from mechanical and electrostatic mechanisms resist external pressures on the TM (Fig. 1). The mechanical component is proportional to changes in TM volume and may be expressed as

$$p_{mech} = \frac{\kappa(V - V_0)}{V_0}, \quad [1]$$

where p_{mech} is the hydraulic pressure, κ is the bulk modulus, V is TM volume, and V_0 is the volume in the absence of a hydraulic pressure. The electrostatic component depends on the concentration of fixed charge in the TM, which tends to concentrate mobile counterions to maintain electroneutrality. This concentration of counterions increases the osmotic pressure (p_{elec}) in the TM and may be expressed as

$$p_{elec} = RT \left(\sqrt{\left(\frac{c_f}{2}\right)^2 + C^2} - C \right), \quad [2]$$

where R is the molar gas constant, T is absolute temperature, and C represents the concentration of monovalent ionic species (KCl) in the bath. This model predicts that electrostatic repulsion due to the -7.1 mmol/L of fixed charge density may contribute up to 0.35 kPa to the equilibrium bulk modulus κ , accounting for $\sim 70\%$ of compressive rigidity of the TM at equilibrium (21). Under dynamic conditions, the contribution of charge to mechanical properties also is important. A recent study found that a shift to acidic pHs in the bath causes about a two- to threefold reduction in dynamic shear impedance of the TM (42). The density of charge in the TM thus is sufficient to be the basis of mechanical properties under both static and dynamic conditions, a striking finding given the fact that the TM is highly hydrated (27, 29, 30).

The presence of charge in the TM suggests the possibility that electrical stimuli might generate a mechanical response (43, 44). The application of oscillating electric fields at audio frequencies (1–1,000 Hz) directed along the transverse axis of the TM in the microaperture chamber (Fig. 3A) generated displacements of the TM near the marginal zone and Hensen's stripe ($n = 4$ TM preparations) (Movie S1). Fig. 3B shows that TM displacements had peak amplitudes of 50 nm in response to 8 kV/m (at 10 Hz) at a position on the undersurface of the TM above the microaperture. Displacement amplitudes dropped significantly with distance away from the microaperture (Fig. 3B), increased with electric field strength (Fig. 3C), and decreased as a function of stimulus frequency with the phase angle approaching $-\pi/2$ radians (Fig. 3D), consistent with viscous dominated interactions. Similar motion behaviors were reproduced in a microfluidics chamber used to apply radial electric fields (SI Materials and Methods, Movie S2, and Fig. S1). Using this chamber, we measured the frequency response of the TM at very low frequencies (1–80 Hz)

and exposed the TM to different perfusates in the microchannel environment. Perfusion of AE equilibrated at pH 3.5 led to a shift in phase angle of $\sim \pi$ radians (Fig. S24), indicating ionization of positively charged collagen groups (38) and neutralization of negatively charged GAGs.

The frequency dependence of TM displacement magnitude and phase (Fig. 3D and Fig. S2B) suggests an interplay between electrophoretic forces on the solid matrix and electro-osmotic forces on interstitial fluid (which carries a charge equal in magnitude but opposite in polarity to the fixed charge on TM macromolecules) (40). At low frequencies, these forces displace the fixed-charge groups attached to the elastic matrix of the TM to generate displacements, which scale with field strength and the radius of the microaperture (45). However, this process is viscosity limited (Fig. 3D) because of the small size of the pores (21). Therefore, as the frequency of the electrical stimulus increases, there is less time per period for fluid motion through the porous matrix and a proportional reduction in total fluid transport. The result is that electrokinetic displacements of the TM are larger at low frequencies than at high frequencies.

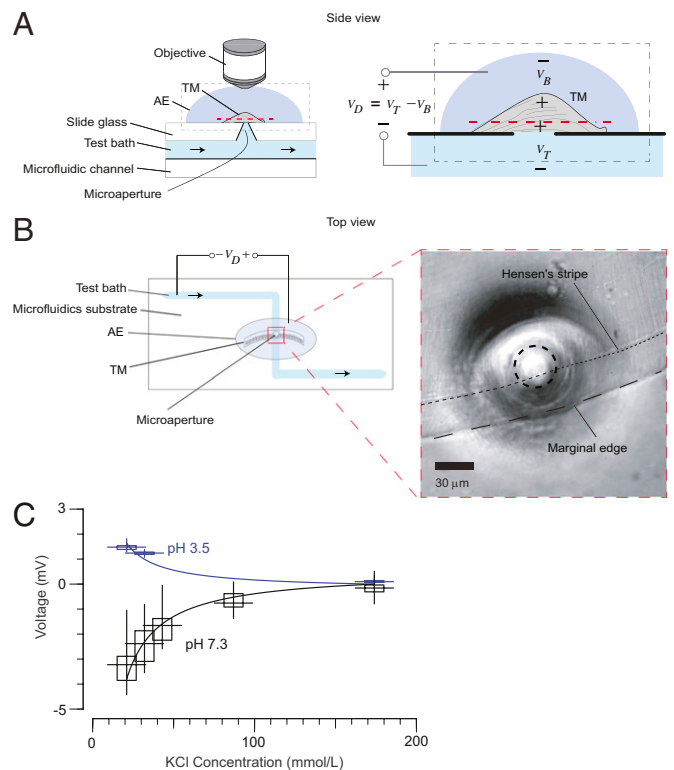


Fig. 2. Fixed-charge density of the TM. (A) Schematic drawings of the microaperture setup showing side views of an isolated TM positioned over a circular microaperture. (Left) The microaperture creates a fluid path from the overlying bath of AE to the underlying microfluidics channel (test bath) perfused with AE-like solutions with variable KCl concentrations. (Right) The TM acts as an electrochemical barrier between the overlying bath and underlying fluid channel. The potential difference between the baths ($V_D = V_T - V_B$) was recorded with Ag/AgCl electrodes that were placed in contact with the two baths. (B) Schematic drawing of the microaperture setup showing the top view of the TM positioned over the microaperture in the region near Hensen's stripe and the marginal zone. (Inset) TM segment overlying the microaperture using 40 \times magnification. (C) Voltage was plotted as a function of test bath KCl concentration. Best-fit estimates to the median voltages yielded c_f (-7.1 ± 2.0 mmol/L; $n = 5$ TM preparations). Vertical lines and boxes denote extreme values and the extent of the interquartile range, respectively. Horizontal lines through the boxes denote the median values. Reducing the bath pH from 7.3 to 3.5 caused voltage measurements to change polarity and decrease in magnitude (3.0 mmol/L).

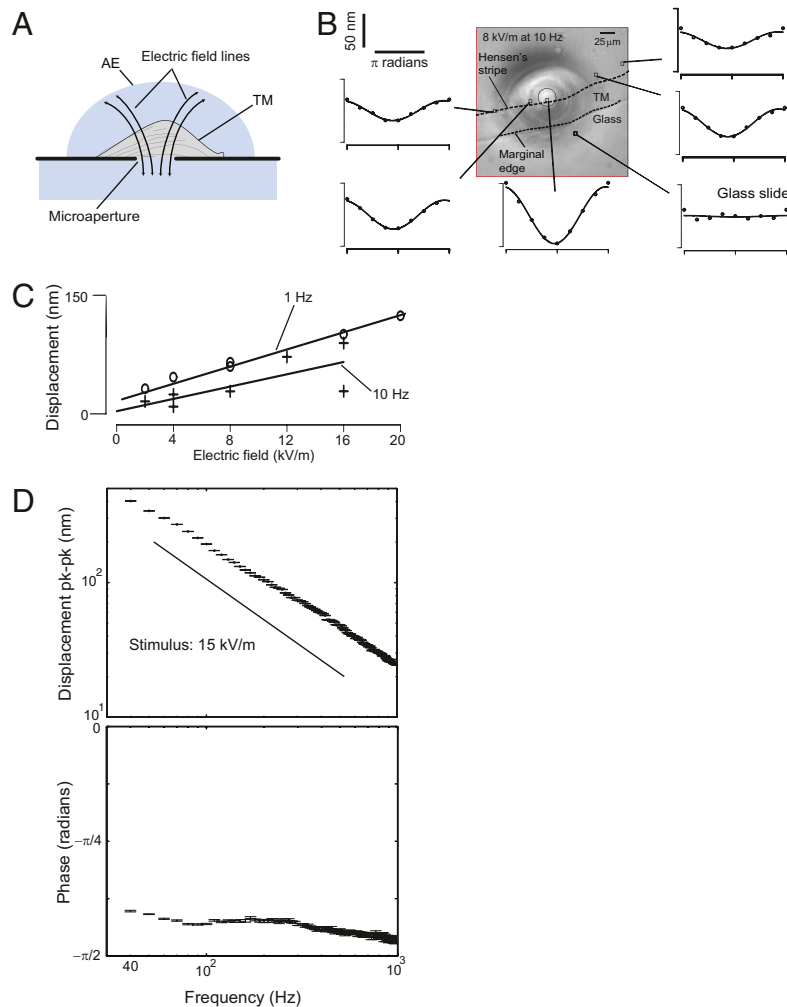


Fig. 3. TM electrokinetic response. (A) The microaperture setup was used to deliver electric fields to the TM with a pair of Ag/AgCl-stimulating electrodes. Electrically evoked displacements were measured using computer microvision and DOCM systems (*Materials and Methods*). Voltages were delivered with Ag/AgCl electrodes positioned in the top bath and in a reservoir connecting to the underlying fluid channel. Electric fields were computed based on the geometry of the microaperture, and electrical current was measured across a resistor that was placed in series with the microaperture chamber during voltage application. (B) Transverse displacements were sinusoidal and largest in the regions of the TM directly overlying the microaperture and decreased with radial distance away from the microaperture. A typical TM segment excised from the middle turn exhibited electrically evoked displacements up to ~45 nm in response to electrical stimuli applied in the middle zone region directly overlying the microaperture (10 Hz; 8 kV/m). Motion amplitudes varied depending on whether the TM sample was a basal or an apical segment. (C) Displacements scaled linearly with electric field magnitude for TM samples excised from the middle turn of the cochlea ($n = 4$ TM preparations). (D) (*Upper*) Displacement amplitudes decreased with increasing stimulus frequency (40–1,000 Hz) with a slope of -1 (solid line) for a typical apical TM segment. Black dots denote the mean value of TM displacement. (*Lower*) Phase angle of TM displacement as a function of frequency. Vertical lines with horizontal bars denote SEM.

For asymptotically low frequencies, the solid and fluid phases separate, and electrokinetic displacements result from electrical forces acting on fixed charges embedded in the elastic matrix. To estimate the magnitude of these displacements, we modeled the TM as a semi-infinite, isotropic, elastic matrix, which overlies a circular aperture (25- μm diameter) through which current is passed. The mechanical properties of the matrix were represented by Young's modulus ($\sim 10^5$ Pa for a basal TM segment) (18, 23). The matrix was assumed to have a uniform electrical resistivity (0.3 $\Omega\cdot\text{m}$) and fixed charge density q ($\sim 7 \times 10^5$ C/m 3), determined from the measurements in this study ($c_f \sim 7$ mmol/L; Fig. 2). The equations of motion were solved using finite differences (*SI Results*), with the result that electric fields of 1 kV/m (generated by ~ 2 μA of current) produced electrokinetic displacements on the order of 1.5 μm . This motion estimate is based on a quasistatic model of the TM, which is appropriate at asymptotically low frequencies. However, the motion measurements in Fig. 3D show strong frequency dependence of motion (with slope of -1) over the

measured range of frequencies (which is limited at low frequencies by table vibrations and thermal drift). We expect the trend shown in Fig. 3D to continue (to lower frequencies) until the transition to quasistatic behavior occurs, at frequencies that correspond to the poroelastic relaxation time [which is on the order of tens of minutes, based on previous osmotic experiments (21, 27)]. Thus, the transition frequency is two to three orders of magnitude below our lowest measured frequency, and we expect the quasistatic motion estimate to be two to three orders of magnitude larger than the measured range of motions.

Under dynamic conditions, viscous forces increasingly couple electro-osmotic and electrophoretic forces, which are equal in magnitude but opposite in direction. To test the effect of pore size and interstitial fluids on TM electrokinetics, we measured TM motion in response to changes in viscosity by introducing different-sized PEG molecules in AE (*SI Results and Materials and Methods*). We altered the viscosity of the fluid surrounding the TM by perfusing AE mixed with large PEG molecules (10 $\mu\text{mol/L}$,

400 kDa), which could not penetrate the TM. To alter internal viscosity of the TM, we perfused AE mixed with small PEG molecules (10 mmol/L, 8 kDa), whose radius of gyration was sufficiently small to enter through TM nanopores (21). Adding small PEG molecules caused TM motion to decrease by ~ 6.5 times, whereas, adding large PEG molecules caused relatively minor changes in TM motion (Fig. S2C). Changing internal viscosity of the TM is functionally equivalent to reducing TM pore size, suggesting a strong dependence of TM electrokinetic interactions on effective porosity and a weak dependence on external viscosity of the surrounding fluid. These results provide a framework for a general poroelastic model of the TM under both quasistatic (21) and dynamic conditions, thereby highlighting the important interplay between fixed-charge groups, porosity, and the internal water content of the TM at the nanoscale.

Electrically evoked displacements of the TM may have important implications for electrical stimulation of the cochlea (46–50). Mechanical responses to electrical stimulation generally have been attributed to OHC somatic and hair bundle motility mechanisms. Although exogenous application of electrical currents undoubtedly excites sensory receptor cells, our results suggest that electrically induced TM motions also must be taken into account if electrical currents flow through the TM. Thus, electrically evoked motions of the cochlear partition may be stimulated at least partially by TM electrokinetics, especially at low audio frequencies.

Electrokinetic properties of the TM might interact directly with hair cell ion channels. Although the exact position of hair cell transduction channels relative to the TM remains unclear, it is well known that the undersurface of the TM is close (nanometer-scale separation) to the tallest rows of stereocilia (51–53). Fig. 4A and B shows the TM–hair bundle interface and highlights how transduction currents, driven predominantly by potassium and calcium ions, generate electric fields, which in turn might exert local force on TM macromolecules. Although it is unlikely that transduction currents generate bulk movements of the TM *in vivo*, it is possible that local electrically induced deformations of the TM might occur near single stereocilia ion channels.

A previous study of electrical recordings from a bullfrog's sacculus found electric field magnitudes of ~ 1 V/m at distances ~ 1 μm from the tips of the stereociliary hair bundles containing clusters of ion channels (51). These electric fields depend not only on the magnitude of the current but also on the spatial proximity of the TM relative to the ion channels. If we assume ~ 20 -pA transduction currents through a solitary ion channel (54, 55) and a distance of ~ 1 μm from the channel opening, the electric fields would be in the range of those measured by Hudspeth (labeled “Ref. 51” in Fig. 4C). However, as the distance to the ion channel is decreased, the field strength increases rapidly. For example, at distances within 7–30 nm of an ion channel, the field strengths are 10^3 – 10^4 V/m, similar to those applied in the microaperture chamber (labeled “This study” in Fig. 4C).

Electrically evoked TM motions and forces produced by transduction electric fields depend on the material properties of the TM as well as the channel geometry. If we assume that a solitary ion channel is modeled as a single nanopore, then we can estimate the magnitude of TM displacements by scaling the measurements in the microaperture setup (Fig. 3). TM motion in the microaperture setup under quasistatic conditions ($d_\mu \sim 1.5$ μm) is proportional to the applied electric field strength ($E_\mu \sim 10^3$ V/m), where the proportionality constant is the effective charge (q_μ) divided by TM stiffness (k_μ). The stiffness k_μ scales with the radius of the microaperture (45) and therefore is $\sim 10^4$ smaller near an ion channel (~ 1 -nm radius), whereas the quantity of charge q_μ scales with the volume of the TM overlying the microaperture. As a result, the proportionality between d_μ and E_μ changes by a factor of 10^8 for a single ion channel relative to the microaperture. On that basis, we predict TM displacements (d_{ch}) near an ion channel to be ~ 0.01 nm in response to E_{ch} adjacent to a nanochannel (Fig.

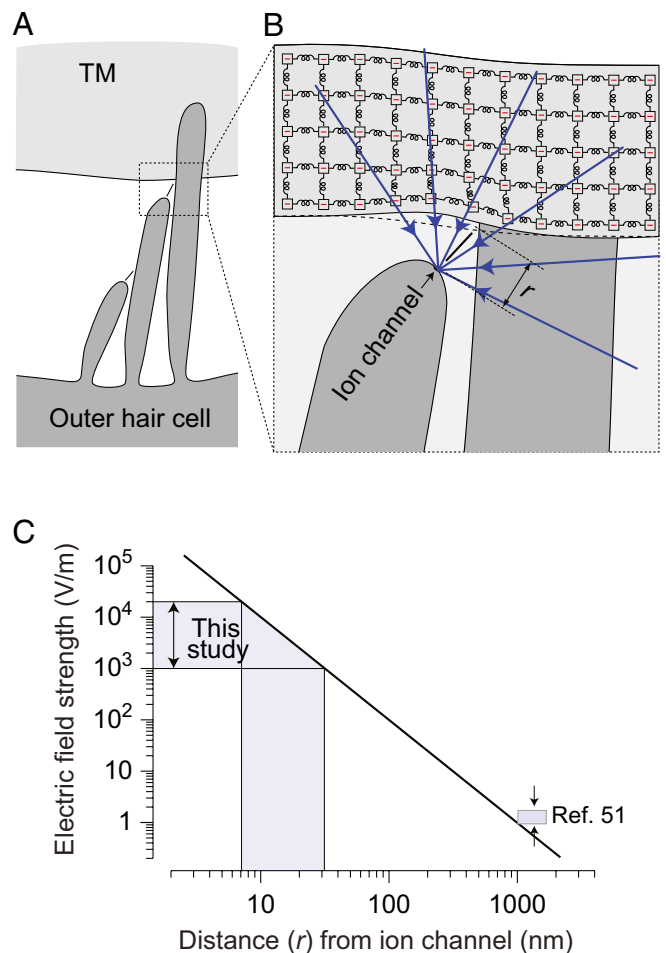


Fig. 4. TM electrokinetics near hair cell ion channels. (A) Schematic drawing of a cochlear partition showing the orientation of the TM relative to OHC stereocilia and tip links. (B) Inset shows the OHC ion channel as a point source with radial electric fields (blue arrows) acting on TM fixed-charge macromolecules locally over small distances r . (C) Model predictions of electric field magnitudes as a function of radial distance r from the opening of the ion channel. Electric fields were estimated based on experimental values for single-channel transduction currents, resistivity of the ionic environment, and the radius of the ion channel from previous data (51–55). The shaded region labeled “This study” denotes the range of electric field (10^2 – 10^4 V/m) magnitudes applied in the microaperture chamber with values corresponding to ~ 7 – 30 nm from the ion channel opening. The shaded region labeled “Ref. 51” denotes electric fields (~ 1 V/m) measured at ~ 1 μm from the tips of hair bundles in the bullfrog's sacculus (51). In both cases, radial distances r are significantly larger than the TM's space charge layer thickness (34).

4C). Because the electric field strength depends linearly on the number of stereociliary channels, the aggregate TM motion for ~ 75 channels (d_{hb}) for a given hair bundle would be ~ 0.75 nm. TM displacements at the ion channel and bundle level scale linearly with electrical current I (SI Results). This linear dependence of TM motion on electrical current is consistent with a finite difference model (SI Results), which predicts TM motion estimates on the order of those based purely on scaling.

The total mechanical energy available from TM electrokinetic motions (SI Results) is the product of d_{hb}^2 and TM stiffness ($k_{TM} \sim 1.33$ N/m for a basal TM segment over a 5- μm radius) (18, 23, 45), yielding ~ 0.75 aJ for basal TM segments and on the order of ~ 7.5 aJ for apical TM segments with lower stiffness ($k_{TM} \sim 0.13$ N/m for an apical TM segment over a 5- μm radius) (18, 23, 45). These energy estimates are comparable with the amount of work needed to deflect hair bundles during calcium-driven bundle

motility (~ 2 aJ) and are significantly larger than the work performed against viscosity during bundle movements (~ 0.1 aJ) (56, 57), suggesting that electrically evoked motions of the TM might interact with MET currents of the hair bundles. The direction of TM motion and the associated feedback mechanism at the level of the hair bundles depend on the location of the MET channels. If the ion channels face toward the inhibitory direction of bundle motion (i.e., if they are on the side closest to a shorter stereocilium), the net electric field caused by opening the channels will generate a force that will tend to close the channels, consistent with negative feedback. If, on the other hand, the ion channels face the tallest stereocilium (as in Fig. 4B), the net electric field would force TM negative charge groups in the direction of positive bundle deflection to open more ion channels, as the basis of a positive feedback mechanism for amplification.

Beyond cochlear mechanics, our findings have important implications for all sensory systems, which (with the exception of a few species of lizards) all contain accessory gelatinous structures overlying hair cells. Gels, such as the cupulae and otolithic membranes found in the vestibular system and those covering electrosensory hair cells on the skin of aquatic vertebrates, play a key role in hair cell stimulation (58–60). Much like the TM, these gels are poised to undergo deformations in response to transduction currents. The effect of electrokinetics may be even greater in these sensory systems because their MET channels operate at significantly lower frequencies than those in the cochlea.

Conclusions

Results reported in this study show that the TM contains a high density of fixed charge that contributes to the compressive stiffness of the TM and may generate electrokinetic phenomena. Electrical stimuli applied to the TM evoke nanometer-scale displacements at audio frequencies by exerting force on the solid matrix (fixed-charge macromolecules) and fluid phase of the TM. This motion is directly related to the density of fixed charge inside the TM and may have important implications for cochlear mechanisms. Although the exact proximity of hair cell ion channels relative to the TM is not well known, the electric fields generated by MET are large near the undersurface of the TM and thus may generate local nanometer-scale deformations of the TM *in vivo*. TM electrokinetic properties thus may play an important role in the deflection of cochlear hair bundles, suggesting, more broadly, that electrokinetic mechanisms may control the interaction of overlying gels and hair bundles in all sensory systems.

Materials and Methods

Isolated TM Preparation. TM segments were excised from the cochleae of adult male mice (strain CD-1, 4–8 wk old; Taconic) using a previously published surgical technique (61). The cochlea was surgically removed and placed in an AE bath containing 174 mM KCl, 5 mM Hepes, 3 mM dextrose, 2 mM NaCl, and 0.02 mM CaCl₂. The bath was equilibrated at pH 7.3 at room temperature. The bone casing of the cochlea was chipped away gently until the organ of Corti was exposed. A combination of bright- and dark-field illumination with a dissection microscope (Zeiss) provided visual access to the TM above the organ of Corti. A sterilized eyelash was used to gently lift the TM from the cochlea. TM segments (typically 0.5–1 mm in length) were isolated from the organ and placed in a fresh AE bath. The care and use of animals in this study were approved by the Massachusetts Institute of Technology Committee on Animal Care.

Microaperture Chamber. The microaperture chamber contained a glass-drilled microaperture (12.5- μ m radius) (Lenox Laser) connecting two fluid-filled compartments in the form of a microchannel and an overlying bath (Fig. 2A). The underlying microchannel was cast in a transparent elastomer called poly(dimethylsiloxane) (PDMS; Sylgard 184; Dow Corning) by applying a standard soft lithography technique (62) in which a PDMS replica of the underlying channel was cured and subsequently sealed to a glass slide containing the microaperture. For fixed-charge density measurements, the top bath was perfused with AE and the microchannel was perfused with AE-like solutions in which the KCl concentration and pH were varied. KCl concentrations of

21 mM, 32 mM, 43 mM, 87 mM, and 174 mM were used at pH 7.3 and 3.5. Each test bath was perfused twice to test for repeatability. For electrokinetic measurements, the top bath and microchannel both were perfused with AE.

Measuring Fixed-Charge Density c_f . Isolated TM segments were mounted in the microaperture chamber so that an electrochemical barrier separating the solutions in the two compartments was formed (Fig. 2A). The DC voltage difference (V_D) between the two compartments was measured with Ag/AgCl microelectrodes (A-M Systems) housed in large-tip micropipettes containing 3 M KCl solution and solidified in agarose. The electrodes were positioned in the top bath and in the reservoir connecting to the microchannel. This configuration allowed uniform electric fields to be delivered in the regions of the TM directly overlying the microaperture. The electrodes were coupled through an amplifier (DAM60-G Differential Amplifier, World Precision Instruments) and a multimeter (TX3 True RMS Multimeter, Tektronix) connected to a computer. DC potentials were stored in the computer at 2-s intervals. The DC potential difference between the two baths depends on the ionic concentration of the two baths and on TM fixed-charge density in this configuration. Therefore, by measuring the electric potential difference across the TM, we can estimate TM fixed-charge density. The potential difference arises primarily from Donnan potentials that form between each bath and the TM as a result of the presence of fixed charge. The potential between each bath and the TM is

$$V = \frac{RT}{F} \left(\sqrt{\left(\frac{c_f}{2C_\Sigma} \right)^2 + 1} + \frac{c_f}{2C_\Sigma} \right), \quad [3]$$

where V is the potential of the TM relative to the bath; R is the molar gas constant; T is absolute temperature; F is Faraday's constant; c_f is the concentration of fixed charge within the TM, which may be either a positive or negative quantity; and $C_\Sigma = (1/2)\Sigma c_i$ is one half the sum of the concentrations c_i of each ion in the bath. Because the bath consisted mainly of KCl, we estimated $C_\Sigma = (1/2)(c_K + c_{Cl})$. If the two baths have identical compositions, the Donnan potential between the TM and each bath is identical, so the net potential difference between baths is zero. If one bath has a lower ionic concentration, the magnitude of the Donnan potential increases, so the potential difference between baths deviates from zero in a manner that depends on c_f within the TM. When the two baths have dissimilar ionic strengths, in addition to the Donnan potential, a liquid junction potential (LJP) may arise between the baths. To measure the Donnan potential accurately, it is important to minimize and measure the LJP. In this respect, it is convenient that the TM normally resides in AE, which consists primarily of K⁺ and Cl[−]. Because these two ions have similar mobilities, the junction potential resulting from a concentration difference between baths is minimized.

Measuring Electrokinetic Motion of the TM. The microaperture setup also was used to apply voltages to TM segments. Isolated TM segments were placed over a microaperture with a radius of ~ 12.5 μ m, and both compartments were perfused with AE. Sinusoidal voltages applied between the compartments generated electric fields in the middle and marginal zones of the TM covering the aperture (Fig. 3 A and B). Displacements were visualized transversely across multiple focal planes within the bulk of the TM using computer vision and Doppler optical coherence microscopy (DOCM) techniques (18, 63).

We also developed a microfluidics chamber (Fig. S1) used to apply electric fields to the TM in the radial (in-plane) direction (*SI Materials and Methods*) (44). Fluids were perfused through the microfluidics chamber, allowing equilibration of AE at different pHs and with PEG (Fig. S2 A and C) for TM motion amplitude, phase, and polarity studies.

Motion Analysis with the Computer Vision System. Images of the TM were collected optically with a 40 \times water immersion objective (0.8 N.A., Zeiss Axioplan) and a transmitted light condenser (0.8 N.A.). TM motion was measured with a 12-bit, 1,024 \times 1,024-pixel CCD camera (CAD7-1024A; Dalsa Inc.) by strobing the light-emitting diode. The TM segment was illuminated at 16 evenly spaced stimulus phases (over a stimulus cycle) at multiple optical planes separated by 1 μ m. The collected images then were analyzed to determine the first eight harmonics of the periodic motion. We computed the magnitude and phase of radial displacement from the series of collected images by using previously published motion-tracking algorithms (18, 20).

Motion Analysis with DOCM. TM electrically evoked motions in the microaperture chamber were confirmed using a previously published DOCM system, which reconstructs motion from weakly scattering light reflected from multiple axial depths through the TM (63). The DOCM system has subnanometer resolution and was used to characterize TM motion as a function of stimulus frequencies.

ACKNOWLEDGMENTS. We thank A. Grodzinsky and J. Guinan for helpful discussions about the manuscript. This research was supported by National Institutes of Health Grant R01-DC00238. R.G. was supported in part by

a training grant from the National Institutes of Health to the Speech and Hearing Bioscience and Technology Program of the Harvard-MIT Division of Health Sciences and Technology.

1. Kössl M, Russell IJ (1995) Basilar membrane resonance in the cochlea of the mustached bat. *Proc Natl Acad Sci USA* 92(1):276–279.
2. Hudspeth AJ (1985) The cellular basis of hearing: The biophysics of hair cells. *Science* 230(4727):745–752.
3. Hudspeth AJ (1989) How the ear's works work. *Nature* 341(6241):397–404.
4. Legan PK, et al. (2000) A targeted deletion in α -tectorin reveals that the tectorial membrane is required for the gain and timing of cochlear feedback. *Neuron* 28(1):273–285.
5. Legan PK, et al. (2005) A deafness mutation isolates a second role for the tectorial membrane in hearing. *Nat Neurosci* 8(8):1035–1042.
6. Russell IJ, et al. (2007) Sharpened cochlear tuning in a mouse with a genetically modified tectorial membrane. *Nat Neurosci* 10(2):215–223.
7. Suzuki N, et al. (2005) Type IX collagen knock-out mouse shows progressive hearing loss. *Neurosci Res* 51(3):293–298.
8. McGuirt WT, et al. (1999) Mutations in COL11A2 cause non-syndromic hearing loss (DFNA13). *Nat Genet* 23(4):413–419.
9. Davis H (1957) Biophysics and physiology of the inner ear. *Physiol Rev* 37(1):1–49.
10. Dallos P, Billone MC, Durrant JD, Wang C, Raynor S (1972) Cochlear inner and outer hair cells: Functional differences. *Science* 177(4046):356–358.
11. Billone M, Raynor S (1973) Transmission of radial shear forces to cochlear hair cells. *J Acoust Soc Am* 54(5):1143–1156.
12. Neely ST, Kim DO (1983) An active cochlear model showing sharp tuning and high sensitivity. *Hear Res* 9(2):123–130.
13. Neely ST, Kim DO (1986) A model for active elements in cochlear biomechanics. *J Acoust Soc Am* 79(5):1472–1480.
14. Allen JB (1980) Cochlear micromechanics—a physical model of transduction. *J Acoust Soc Am* 68(6):1660–1670.
15. Zwislocki JJ (1980) Five decades of research on cochlear mechanics. *J Acoust Soc Am* 67(5):1679–1685.
16. Mammano F, Nobili R (1993) Biophysics of the cochlea: Linear approximation. *J Acoust Soc Am* 93(6):3320–3332.
17. Zwislocki JJ (1979) Tectorial membrane: A possible sharpening effect on the frequency analysis in the cochlea. *Acta Otolaryngol* 87(3-4):267–269.
18. Ghaffari R, Aranyosi AJ, Freeman DM (2007) Longitudinally propagating traveling waves of the mammalian tectorial membrane. *Proc Natl Acad Sci USA* 104(42):16510–16515.
19. Meaud J, Grosh K (2010) The effect of tectorial membrane and basilar membrane longitudinal coupling in cochlear mechanics. *J Acoust Soc Am* 127(3):1411–1421.
20. Ghaffari R, Aranyosi AJ, Richardson GP, Freeman DM (2010) Tectorial membrane travelling waves underlie abnormal hearing in Tectb mutant mice. *Nat Commun* 1:96.
21. Masaki K, Weiss TF, Freeman DM (2006) Poroelectric bulk properties of the tectorial membrane measured with osmotic stress. *Biophys J* 91(6):2356–2370.
22. Gavara N, Chadwick RS (2009) Collagen-based mechanical anisotropy of the tectorial membrane: implications for inter-row coupling of outer hair cell bundles. *PLoS ONE* 4(3):e4877.
23. Gueta R, Barlam D, Shneck RZ, Rousso I (2006) Measurement of the mechanical properties of isolated tectorial membrane using atomic force microscopy. *Proc Natl Acad Sci USA* 103(40):14790–14795.
24. Richter CP, Emadi G, Getnick G, Quesnel A, Dallos P (2007) Tectorial membrane stiffness gradients. *Biophys J* 93(6):2265–2276.
25. Richardson GP, Lukashkin AN, Russell IJ (2008) The tectorial membrane: One slice of a complex cochlear sandwich. *Curr Opin Otolaryngol Head Neck Surg* 16(5):458–464.
26. Gavara N, Manoussaki D, Chadwick RS (2011) Auditory mechanics of the tectorial membrane and the cochlear spiral. *Curr Opin Otolaryngol Head Neck Surg* 19(5):382–387.
27. Freeman DM, Masaki K, McAllister AR, Wei JL, Weiss TF (2003) Static material properties of the tectorial membrane: A summary. *Hear Res* 180(1-2):11–27.
28. Masaki K, et al. (2010) Tectorial membrane material properties in Tecta(Y)(1870C+) heterozygous mice. *Biophys J* 99(10):3274–3281.
29. Kronester-Frei A (1978) Sodium dependent shrinking properties of the tectorial membrane. *Scan Electron Microsc* 2:943–948.
30. Thalmann I, et al. (1987) Composition and supramolecular organization of the tectorial membrane. *Laryngoscope* 97(3 Pt 1):357–367.
31. Richardson GP, Russell IJ, Duance VC, Bailey AJ (1987) Polypeptide composition of the mammalian tectorial membrane. *Hear Res* 25(1):45–60.
32. Thalmann I, Machiki K, Calabro A, Hascall VC, Thalmann R (1993) Uronic acid-containing glycosaminoglycans and keratan sulfate are present in the tectorial membrane of the inner ear: Functional implications. *Arch Biochem Biophys* 307(2):391–396.
33. Thalmann I (1993) Collagen of accessory structures of organ of Corti. *Connect Tissue Res* 29(3):191–201.
34. Buschmann MD, Grodzinsky AJ (1995) A molecular model of proteoglycan-associated electrostatic forces in cartilage mechanics. *J Biomech Eng* 117(2):179–192.
35. Kim YJ, Bonassar LJ, Grodzinsky AJ (1995) The role of cartilage streaming potential, fluid flow and pressure in the stimulation of chondrocyte biosynthesis during dynamic compression. *J Biomech* 28(9):1055–1066.
36. Weiss TF, Freeman DM (1997) Equilibrium behavior of an isotropic polyelectrolyte gel model of the tectorial membrane: The role of fixed charges. *Aud Neurosci* 3:351–361.
37. Freeman DM, Hattangadi SM, Weiss TF (1997) Osmotic responses of the isolated mouse tectorial membrane to changes in pH. *Aud Neurosci* 3:363–375.
38. Weiss TF, Freeman DM (1997) Equilibrium behavior of an isotropic polyelectrolyte gel model of the tectorial membrane: Effect of pH. *Hear Res* 111(1-2):55–64.
39. Grodzinsky AJ (1983) Electromechanical and physicochemical properties of connective tissue. *Crit Rev Biomed Eng* 9(2):133–199.
40. Frank EH, Grodzinsky AJ (1987) Cartilage electromechanics—I. Electrokinetic transduction and the effects of electrolyte pH and ionic strength. *J Biomech* 20(6):615–627.
41. Steel KP (1983) Donnan equilibrium in the tectorial membrane. *Hear Res* 12(2):265–272.
42. Farrahi S, Ghaffari R, Freeman DM (2011) Lowered pH alters decay but not speed of tectorial membrane waves. *What Fire Is in Mine Ears: Progress in Auditory Biomechanics. Proceedings of the 11th International Mechanics of Hearing Workshop*, eds. Shera CA, Olson ES (American Institute of Physics, Melville, NY), Vol 1403, pp 403–404.
43. Ghaffari R (2003) Electrically-evoked motions of the isolated mouse tectorial membrane. Master's thesis (Massachusetts Institute of Technology, Cambridge, MA).
44. Ghaffari R (2008) The functional role of the mammalian tectorial membrane in cochlear mechanics. PhD thesis (Massachusetts Institute of Technology, Cambridge, MA).
45. Timoshenko S, Goodier JN (1951) *Theory of Elasticity* (McGraw-Hill, New York).
46. Xue S, Mountain DC, Hubbard AE (1995) Electrically evoked basilar membrane motion. *J Acoust Soc Am* 97(5 Pt 1):3030–3041.
47. Scherer MP, Gummer AW (2004) Vibration pattern of the organ of Corti up to 50 kHz: Evidence for resonant electromechanical force. *Proc Natl Acad Sci USA* 101(51):17652–17657.
48. Chan DK, Hudspeth AJ (2005) Mechanical responses of the organ of Corti to acoustic and electrical stimulation in vitro. *Biophys J* 89(6):4382–4395.
49. Nowotny M, Gummer AW (2006) Nanomechanics of the subreticular space caused by electromechanics of cochlear outer hair cells. *Proc Natl Acad Sci USA* 103(7):2120–2125.
50. Karavitaki KD, Mountain DC (2007) Imaging electrically evoked micromechanical motion within the organ of Corti of the excised gerbil cochlea. *Biophys J* 92(9):3294–3316.
51. Hudspeth AJ (1982) Extracellular current flow and the site of transduction by vertebrate hair cells. *J Neurosci* 2(1):1–10.
52. Fettiplace R, Hackney CM (2006) The sensory and motor roles of auditory hair cells. *Nat Rev Neurosci* 7(1):19–29.
53. Beurg M, Fettiplace R, Nam JH, Ricci AJ (2009) Localization of inner hair cell mechanotransducer channels using high-speed calcium imaging. *Nat Neurosci* 12(5):553–558.
54. Farris HE, LeBlanc CL, Goswami J, Ricci AJ (2004) Probing the pore of the auditory hair cell mechanotransducer channel in turtle. *J Physiol* 558(Pt 3):769–792.
55. Johnson SL, Beurg M, Marcotti W, Fettiplace R (2011) Prestin-driven cochlear amplification is not limited by the outer hair cell membrane time constant. *Neuron* 70(6):1143–1154.
56. Choe Y, Magnasco MO, Hudspeth AJ (1998) A model for amplification of hair-bundle motion by cyclical binding of Ca^{2+} to mechano-electrical-transduction channels. *Proc Natl Acad Sci USA* 95(26):15321–15326.
57. Breneman KD, Brownell WE, Rabbitt RD (2009) Hair cell bundles: Flexoelectric motors of the inner ear. *PLoS ONE* 4(4):e5201.
58. Freitas R, Zhang GJ, Albert JS, Evans DH, Cohn MJ (2006) Developmental origin of shark electroreceptive organs. *Evol Dev* 8(1):74–80.
59. Bullock TH (1982) Electroreception. *Annu Rev Neurosci* 5:121–170.
60. Rabbitt RD, Boyle R, Highstein SM (2010) Mechanical amplification by hair cells in the semicircular canals. *Proc Natl Acad Sci USA* 107(8):3864–3869.
61. Shah DM, Freeman DM, Weiss TF (1995) The osmotic response of the isolated, unfixed mouse tectorial membrane to isosmotic solutions: Effect of Na^+ , K^+ , and Ca^{2+} concentration. *Hear Res* 87(1-2):187–207.
62. McDonald JC, et al. (2000) Fabrication of microfluidic systems in poly(dimethylsiloxane). *Electrophoresis* 21(1):27–40.
63. Hong SS, Freeman DM (2006) Doppler optical coherence microscopy for studies of cochlear mechanics. *J Biomed Opt* 11(5):054014.